On the impact of model errors on input and state estimation in structural dynamic systems

Petersen, W.; Lourens, E.; Maes, K.

Citation (APA)
Petersen, W., Lourens, E., & Maes, K. (2024). On the impact of model errors on input and state estimation in structural dynamic systems. In W. Desmet, B. Pluymers, D. Moens, & J. del Fresno Zarza (Eds.), *Proceedings of ISMA 2024 - International Conference on Noise and Vibration Engineering and USD 2024 - International Conference on Uncertainty in Structural Dynamics* (pp. 4262-4275). Katholieke Universiteit Leuven.

Important note
To cite this publication, please use the final published version (if applicable).
Please check the document version above.

On the impact of model errors on input and state estimation in structural dynamic systems

Ø. W. Petersen [1]**, E. Lourens** [2]**, K. Maes** [3]
[1] NTNU, Department of Structural Engineering
e-mail: **oyvind.w.petersen@ntnu.no**

[2] TU Delft, Faculty of Civil Engineering and Geosciences

[3] KU Leuven, Department of Civil Engineering, Kasteelpark Arenberg 40, B-3001, Heverlee, Belgium

Abstract

In applied structural dynamics, input and state estimation techniques are used to identify unmeasurable response quantities and unknown forces from limited sensor data. These estimators depend on mechanical state-space models, which can be inaccurate due to uncertainties in the systems' mass, damping, and stiffness (or equivalently, the modal parameters of a linear system). This work examines the impact of such model errors and their effects are characterized by a theoretical framework for error propagation to the estimated quantities. The results are exemplified in a numerical example of a mass-spring system. The characterization is a first step towards more focused attempts to develop algorithms in the realm of input and state estimation that are able to deal more robustly with numerical models subject to uncertainty.

1 Introduction

In recent decades, technology improvements have allowed for the wide deployment of sensors for measuring structural responses. However, not all response quantities are directly measurable in practical applications. To address this, model-based state estimation techniques using limited response data have become widely applied, where the most famous examples are the class of sequential Bayesian filters with a structure similar to the Kalman filter [1]. Extensions to input estimation have also been developed for situations where the forces exerted on the system are unknown [2, 3, 4, 5, 6, 7].

These input and state estimators rely on mechanical state-space models, which in structural dynamics are often constructed from numerically calculated mode shapes, natural frequencies, and damping ratios. However, these numerical models inherently carry uncertainties due to simplifications (e.g., boundary conditions, geometry, or joint stiffness), unknown material parameter values, complicated damping behaviour, etc. The effect of model variability due to environmental influence has also been studied for Kalman filters [8].

Experience has shown that the input and state estimates can be sensitive to these model errors. The impact of model errors on Kalman filter performance has been a topic of discussion since as early as 1966 [9]. Since that time, discussions have continued strongly in the field of numerical weather prediction [10], where insufficient model resolution is an inherent error source. To tackle this problem, ensemble filters are commonly used [11].

Parameter estimation methods can be applied to simultaneously correct for uncertain parameters. Examples in structural dynamics can be found in [12, 13, 14]. However, this usually requires specific model component(s) to be selected as targets for updating, which can leave other uncertainties unaddressed. Adaptive covariance methods have also been proposed in many forms, where the earliest works addressing these approaches can be found in [15, 16]. Although most Bayesian filter techniques incorporate uncertainties in the form of additive Gaussian white noise, these uncertainties fail to explicitly account for model errors characterized by non-white residuals and strong noise correlations.

This contribution investigates the impact of such model errors on the results of common linear input and state estimation filters. The effects are characterized from a theoretical standpoint, and the influence of modal parameter errors is also discussed.

2 Theoretical perspective

2.1 Linear state-space models

For linear problems, sequential Bayesian filters typically utilize stochastic-deterministic system models. In this regard, conventional state-space model representations are employed:

$$\mathbf{x}_{k+1} = \mathbf{A}\mathbf{x}_k + \mathbf{B}\mathbf{p}_k + \mathbf{w}_k \tag{1}$$

$$\mathbf{y}_k = \mathbf{G}\mathbf{x}_k + \mathbf{J}\mathbf{p}_k + \mathbf{v}_k \tag{2}$$

Here, the noise covariance matrices are defined as $\mathbb{E}[\mathbf{w}_k\mathbf{w}_k^\mathrm{T}] = \mathbf{Q}$, $\mathbb{E}[\mathbf{v}_k\mathbf{v}_k^\mathrm{T}] = \mathbf{R}$, and $\mathbb{E}[\mathbf{w}_k\mathbf{v}_k^\mathrm{T}] = \mathbf{S}$. For an elaboration of the symbols and notations in the construction of state-space models given below, we refer to the many papers where this is explained [2, 3], and details are omitted here.

Eqs. (1) and (2), which is referred to as the true model, is assumed to be free of errors, thereby serving as a benchmark reference for comparison with erroneous models later on. The model in Eqs. (1) and (2) may be constructed in various ways, and the theoretical derivations provided in this contribution apply to a general model $(\mathbf{A}, \mathbf{B}, \mathbf{G}, \mathbf{J})$, which may be generated using the finite element method or even through data-driven identification. For simplicity, modal coordinates with proportional damping and real mode shapes are hereafter used as an example. To this end, the system dynamics are described by an error-free modal equation of motion:

$$\ddot{\mathbf{z}}(t) + 2\boldsymbol{\Omega}\boldsymbol{\Xi}\dot{\mathbf{z}}(t) + \boldsymbol{\Omega}^2\mathbf{z}(t) = \boldsymbol{\Phi}^\mathrm{T}\mathbf{S}_\mathrm{p}\mathbf{p}(t) \tag{3}$$

Under the assumption of a zero-order hold on the input, the transformation to discrete state-space form is given as:

$$\mathbf{A} = \exp\left(\begin{bmatrix} \mathbf{0} & \mathbf{I} \\ -\boldsymbol{\Omega}^2 & -2\boldsymbol{\Omega}\boldsymbol{\Xi} \end{bmatrix}\Delta t\right), \quad \mathbf{B} = (\mathbf{A} - \mathbf{I})\begin{bmatrix} -\boldsymbol{\Omega}^2\boldsymbol{\Phi}^\mathrm{T}\mathbf{S}_\mathrm{p} \\ \mathbf{0} \end{bmatrix} \tag{4}$$

For a linear output vector $\mathbf{y}(t) = \mathbf{S}_\mathrm{a}\boldsymbol{\Phi}\ddot{\mathbf{z}}(t) + \mathbf{S}_\mathrm{v}\boldsymbol{\Phi}\dot{\mathbf{z}}(t) + \mathbf{S}_\mathrm{d}\boldsymbol{\Phi}\mathbf{z}(t)$ that contains accelerations, velocities, or displacements, respectively, the corresponding system matrices are given by:

$$\mathbf{G} = \begin{bmatrix} \mathbf{S}_\mathrm{d}\boldsymbol{\Phi} - \mathbf{S}_\mathrm{a}\boldsymbol{\Phi}\boldsymbol{\Omega}^2 & \mathbf{S}_\mathrm{v}\boldsymbol{\Phi} - \mathbf{S}_\mathrm{a}\boldsymbol{\Phi}2\boldsymbol{\Omega}\boldsymbol{\Xi} \end{bmatrix}, \quad \mathbf{J} = \begin{bmatrix} \mathbf{S}_\mathrm{a}\boldsymbol{\Phi}\boldsymbol{\Phi}^\mathrm{T}\mathbf{S}_\mathrm{p} \end{bmatrix} \tag{5}$$

The model input-to-output transfer function of Eq. (1) and (2), which will be used later, is given as follows:

$$\mathbf{H}_{\mathbf{yp}}(\omega) = \mathbf{G}\big(\exp(i\omega\Delta t)\mathbf{I} - \mathbf{A}\big)^{-1}\mathbf{B} + \mathbf{J} \tag{6}$$

These transfer functions exhibit resonance at the natural frequencies of the modes, but also contain anti-resonances. While natural frequencies are global properties (i.e., a universal characteristic of a mode), anti-resonance frequencies in a transfer function are local features that depend on the specific input and output locations. This dependency arises due to the local mode shape values. The transfer function between a single displacement u and the force p can be expressed as [17]:

$$H(\omega) = \sum_{m=1}^{N} \frac{A_{ij}^{(m)}}{-\omega^2 + i\omega 2\xi_m\omega_m + \omega_m^2} \tag{7}$$

Here, $A_{ij}^{(m)} = \phi_{im}\phi_{jm}$ is the modal product of between the mode shape value in the degrees of freedom (DOFs) i for the output and j for the input. Anti-resonances are characterized by minima in the transfer function. However, not all minima qualify as anti-resonances; anti-resonances exhibit a sharp dip and not a shallow depression. For further details, please refer to the figures in later examples (Section 3) and literature

on this subject [17, 18, 19]. If instead an acceleration output is considered, the transfer function will be scaled by ω^2, but the anti-resonance frequencies will not change. See [20] for a review of the change of anti-resonances to structural modifications (which, in a broader context, also applies to numerical model modifications).

2.2 Problem formulation for model errors

Now consider the inevitable situation where model errors are present. In general, the following convention is adopted for an arbitrary quantity $\mathbf{X}$:

$$\mathbf{X} = \mathbf{X}_e + \Delta\mathbf{X} \tag{8}$$

Here, $\mathbf{X}$ is the true value and the subscript $(\cdot)_e$ (or superscript $(\cdot)^e$) denotes erroneous quantities. The delta term is the error or perturbation. Now examine the case when a modal model is built using erroneous matrices $\mathbf{\Omega}_e$, $\mathbf{\Xi}_e$, and $\mathbf{\Phi}_e$. Eq. (3) can be rewritten as follows:

$$\ddot{\mathbf{z}} + 2(\mathbf{\Omega}_e + \Delta\mathbf{\Omega})(\mathbf{\Xi}_e + \Delta\mathbf{\Xi})\dot{\mathbf{z}} + (\mathbf{\Omega}_e + \Delta\mathbf{\Omega})^2\mathbf{z} = (\mathbf{\Phi}_e + \Delta\mathbf{\Phi})^{\mathrm{T}}\mathbf{S}_{\mathrm{p}}\mathbf{p} \tag{9}$$

After neglecting higher-order delta terms (e.g. $\Delta\mathbf{\Omega}\Delta\mathbf{\Xi}$) and rearranging, the governing equation can be written as:

$$\underbrace{\ddot{\mathbf{z}}(t) + 2\mathbf{\Omega}_e\mathbf{\Xi}_e\dot{\mathbf{z}}(t) + \mathbf{\Omega}_e^2\mathbf{z}(t) = \mathbf{\Phi}_e^{\mathrm{T}}\mathbf{S}_{\mathrm{p}}\mathbf{p}(t)}_{\text{Modeled dynamics}} \quad \underbrace{+ \Delta\mathbf{\Phi}^{\mathrm{T}}\mathbf{S}_{\mathrm{p}}\mathbf{p}(t) - 2\mathbf{\Omega}_e\Delta\mathbf{\Omega}\mathbf{z}(t) - (2\mathbf{\Omega}_e\Delta\mathbf{\Xi} + 2\mathbf{\Xi}_e\Delta\mathbf{\Omega})\dot{\mathbf{z}}(t)}_{\text{Unmodeled force residual}} \tag{10}$$

Here, the first part (called "Modeled dynamics") is what is perceived as the system equations if the presence of model errors is naively discarded. As expected, there is also a force residual dependent on $\Delta\mathbf{\Omega}$, $\Delta\mathbf{\Xi}$, and $\Delta\mathbf{\Phi}$. When the erroneous model is used in the Bayesian filters, a disparity emerges between model predictions and actual measurements. Due to this imbalance, the erroneous model feels as if the unmodeled force residual is an input applied to the system. Some methods propose to compensate for the model errors by, for instance, inflating the noise covariance matrices $\mathbf{Q}$, $\mathbf{R}$, and $\mathbf{S}$ [21]. Even when erroneous models are used in the present work, however, these covariance matrices are assigned their nominal values in order to study the influence of system model errors in isolation. A study of mismatched noise covariances was performed in [22].

2.3 Impact of model errors: state estimation

The case of pure state estimation using the linear Kalman filter is considered first. The deterministic input force $\mathbf{p}(t)$ is assumed to be fully known (or simply zero). While this can be difficult in practice, this simplification is introduced to avoid additional error terms in the derivations. Still, it should be remarked that the derivations in this section also apply to methods such as the augmented Kalman filter [3], where the unknown force is augmented into the states and thus is treated as a state estimation problem.

The propagation of model errors to state estimates can be analysed by assuming that the Kalman filter operates in the steady state, which is often the case for practical structural dynamic problems. The Kalman filter equations may be summarised as follows [23]:

Measurement update:

$$\bar{\mathbf{R}} = \mathbf{G}\mathbf{P}^{(-)}\mathbf{G}^{\mathrm{T}} + \mathbf{R} \tag{11}$$

$$\hat{\mathbf{x}}_{k|k} = \hat{\mathbf{x}}_{k|k-1} + \mathbf{M}(\mathbf{y}_k - \mathbf{G}\hat{\mathbf{x}}_{k|k-1} - \mathbf{J}\mathbf{p}_k) \tag{12}$$

$$\mathbf{M} = \mathbf{P}^{(-)}\mathbf{G}^{\mathrm{T}}\bar{\mathbf{R}}^{-1} \tag{13}$$

$$\mathbf{P} = \mathbf{P}^{(-)} - \mathbf{M}\mathbf{G}\mathbf{P}^{(-)} \tag{14}$$

Time update:

$$\hat{\mathbf{x}}_{k+1|k} = \mathbf{A}\hat{\mathbf{x}}_{k|k-1} + \mathbf{B}\mathbf{p}_k + \mathbf{L}(\mathbf{y}_k - \mathbf{G}\hat{\mathbf{x}}_{k|k-1} - \mathbf{J}\mathbf{p}_k) \tag{15}$$

$$\mathbf{L} = (\mathbf{A}\mathbf{P}^{(-)}\mathbf{G}^{\mathrm{T}} + \mathbf{S})\bar{\mathbf{R}}^{-1} \tag{16}$$

$$\mathbf{P}^{(-)} = \mathbf{A}\mathbf{P}^{(-)}\mathbf{A}^{\mathrm{T}} + \mathbf{Q} - \mathbf{L}(\mathbf{A}\mathbf{P}^{(-)}\mathbf{G}^{\mathrm{T}} + \mathbf{S})^{\mathrm{T}} \tag{17}$$

Here, the matrices $\bar{\mathbf{R}}$, $\mathbf{M}$, and $\mathbf{L}$ are written without time index k since they are stabilized in the steady state. The error covariance matrices $\mathbb{E}[(\mathbf{x}_k - \hat{\mathbf{x}}_{k|k-1})(\mathbf{x}_k - \hat{\mathbf{x}}_{k|k-1})^{\mathrm{T}}] = \mathbf{P}^{(-)}$, and $\mathbb{E}[(\mathbf{x}_k - \hat{\mathbf{x}}_{k|k})(\mathbf{x}_k - \hat{\mathbf{x}}_{k|k})^{\mathrm{T}}] = \mathbf{P}$ are also constant.

Next, it is moved to the frequency-domain representation of the Kalman filter by applying the Fourier transform to Eq. (12) and (15):

$$\hat{\mathbf{x}}(\omega) = \hat{\mathbf{x}}^{(-)}(\omega) + \mathbf{M}(\mathbf{y}(\omega) - \mathbf{G}\hat{\mathbf{x}}^{(-)}(\omega) - \mathbf{J}\mathbf{p}(\omega)) \tag{18}$$

$$\hat{\mathbf{x}}^{(-)}(\omega)\exp(i\omega\Delta t) = \mathbf{A}\hat{\mathbf{x}}^{(-)}(\omega) + \mathbf{B}\mathbf{p}(\omega) + \mathbf{L}(\mathbf{y}(\omega) - \mathbf{G}\hat{\mathbf{x}}^{(-)}(\omega) - \mathbf{J}\mathbf{p}(\omega)) \tag{19}$$

From this, the following frequency-domain relations for the state estimates can be formed:

$$\begin{bmatrix} \hat{\mathbf{x}}(\omega) \\ \hat{\mathbf{x}}^{(-)}(\omega) \end{bmatrix} = \begin{bmatrix} \mathbf{I} & -\mathbf{I} + \mathbf{M}\mathbf{G} \\ \mathbf{0} & \exp(i\omega\Delta t)\mathbf{I} - (\mathbf{A} - \mathbf{L}\mathbf{G}) \end{bmatrix}^{-1} \left(\begin{bmatrix} \mathbf{M} \\ \mathbf{L} \end{bmatrix} \mathbf{y}(\omega) + \begin{bmatrix} -\mathbf{M}\mathbf{J} \\ \mathbf{B} - \mathbf{L}\mathbf{J} \end{bmatrix} \mathbf{p}(\omega) \right) \tag{20}$$

Thus, for the filtered state estimate, the following relation applies:

$$\hat{\mathbf{x}}(\omega) = \mathbf{T}_{\hat{\mathbf{x}}\mathbf{y}}(\omega)\mathbf{y}(\omega) + \mathbf{T}_{\hat{\mathbf{x}}\mathbf{p}}(\omega)\mathbf{p}(\omega) \tag{21}$$

Here, $\mathbf{T}_{\hat{\mathbf{x}}\mathbf{y}}(\omega)$ and $\mathbf{T}_{\hat{\mathbf{x}}\mathbf{p}}(\omega)$ are the filter transfer functions. Next, the output is formulated in the frequency domain:

$$\mathbf{y}(\omega) = \mathbf{H}_{\mathbf{y}\mathbf{p}}(\omega)\mathbf{p}(\omega) + \mathbf{H}_{\mathbf{y}\mathbf{w}}(\omega)\mathbf{w}(\omega) + \mathbf{v}(\omega) \tag{22}$$

This may be inserted into Eq. (21):

$$\begin{aligned} \hat{\mathbf{x}}(\omega) &= \mathbf{T}_{\hat{\mathbf{x}}\mathbf{y}}(\omega)(\mathbf{H}_{\mathbf{y}\mathbf{p}}(\omega)\mathbf{p}(\omega) + \mathbf{H}_{\mathbf{y}\mathbf{w}}(\omega)\mathbf{w}(\omega) + \mathbf{v}(\omega)) + \mathbf{T}_{\hat{\mathbf{x}}\mathbf{p}}(\omega)\mathbf{p}(\omega) \\ &= (\mathbf{T}_{\hat{\mathbf{x}}\mathbf{y}}(\omega)\mathbf{H}_{\mathbf{y}\mathbf{p}}(\omega) + \mathbf{T}_{\hat{\mathbf{x}}\mathbf{p}}(\omega))\mathbf{p}(\omega) + \mathbf{T}_{\hat{\mathbf{x}}\mathbf{y}}(\omega)\mathbf{H}_{\mathbf{y}\mathbf{w}}(\omega)\mathbf{w}(\omega) + \mathbf{T}_{\hat{\mathbf{x}}\mathbf{y}}(\omega)\mathbf{v}(\omega) \end{aligned} \tag{23}$$

When an erroneous model is employed instead of its true counterpart, the filter transfer functions are also perturbed from their optimal values. For the erroneous case, the state estimate reads:

$$\hat{\mathbf{x}}_e(\omega) = \mathbf{T}_{\hat{\mathbf{x}}\mathbf{y}}^e(\omega)\mathbf{y}(\omega) + \mathbf{T}_{\hat{\mathbf{x}}\mathbf{p}}^e(\omega)\mathbf{p}(\omega) \tag{24}$$

The vector $\Delta\hat{\mathbf{x}} = \hat{\mathbf{x}} - \hat{\mathbf{x}}_e$ quantifies the estimation delta:

$$\Delta\hat{\mathbf{x}}(\omega) = (\Delta\mathbf{T}_{\hat{\mathbf{x}}\mathbf{y}}(\omega)\mathbf{H}_{\mathbf{y}\mathbf{p}}(\omega) + \Delta\mathbf{T}_{\hat{\mathbf{x}}\mathbf{p}}(\omega))\mathbf{p}(\omega) + \Delta\mathbf{T}_{\hat{\mathbf{x}}\mathbf{y}}(\omega)\mathbf{H}_{\mathbf{y}\mathbf{w}}(\omega)\mathbf{w}(\omega) + \Delta\mathbf{T}_{\hat{\mathbf{x}}\mathbf{y}}(\omega)\mathbf{v}(\omega) \tag{25}$$

where $\Delta\mathbf{T}_{\hat{\mathbf{x}}\mathbf{y}}(\omega) = \mathbf{T}_{\hat{\mathbf{x}}\mathbf{y}}(\omega) - \mathbf{T}_{\hat{\mathbf{x}}\mathbf{y}}^e(\omega)$ and $\Delta\mathbf{T}_{\hat{\mathbf{x}}\mathbf{p}}(\omega) = \mathbf{T}_{\hat{\mathbf{x}}\mathbf{p}}(\omega) - \mathbf{T}_{\hat{\mathbf{x}}\mathbf{p}}^e(\omega)$. From Eq. (25), it is clear that the state estimate difference is driven by a frequency-domain transformation of the input force. This transformation may be described by the expression $\Delta\mathbf{T}_{\hat{\mathbf{x}}\mathbf{y}}(\omega)\mathbf{H}_{\mathbf{y}\mathbf{p}}(\omega) + \Delta\mathbf{T}_{\hat{\mathbf{x}}\mathbf{p}}(\omega)$, which is illustrated in later examples (Section 3). A similar transformation of the process noise $\mathbf{w}(\omega)$ and output noise $\mathbf{v}(\omega)$ occurs in Eq. (25) as well.

Finally, it is worth noting that even when a true model is employed, the resulting estimate $\hat{\mathbf{x}}$ remains inherently uncertain due to its Gaussian nature. This uncertainty is quantified by the error covariance matrix $\mathbf{P}$ in Eq. (14). The metric $\Delta\hat{\mathbf{x}}$ therefore quantifies the additional error stemming from the use of an erroneous model.

2.4 Impact of model errors: input and state estimation

Next, the case of joint estimation of inputs and states is considered using the algorithm from [2]. Similar to the Kalman filter, frequency-domain relations for the estimates can be formulated when the filter is run in the steady state:

$$\hat{\mathbf{x}}(\omega) = \mathbf{T}_{\hat{\mathbf{x}}\mathbf{y}}(\omega)\mathbf{y}(\omega) \tag{26}$$

$$\hat{\mathbf{p}}(\omega) = \mathbf{T}_{\hat{\mathbf{p}}\mathbf{y}}(\omega)\mathbf{y}(\omega) \tag{27}$$

The expressions for $\mathbf{T}_{\hat{\mathbf{x}}\mathbf{y}}(\omega)$ and $\mathbf{T}_{\hat{\mathbf{p}}\mathbf{y}}(\omega)$ are given in [5], and omitted here for brevity. When an erroneous model is used, these filter transfer functions take an erroneous form:

$$\hat{\mathbf{x}}_e(\omega) = \mathbf{T}_{\hat{\mathbf{x}}\mathbf{y}}^e(\omega)\mathbf{y}(\omega) \tag{28}$$

$$\hat{\mathbf{p}}_e(\omega) = \mathbf{T}_{\hat{\mathbf{p}}\mathbf{y}}^e(\omega)\mathbf{y}(\omega) \tag{29}$$

The deltas for the state and input estimates may be expressed as follows:

$$\begin{aligned}\Delta\hat{\mathbf{x}}(\omega) = \hat{\mathbf{x}}(\omega) - \hat{\mathbf{x}}_e(\omega) &= \Delta\mathbf{T}_{\hat{\mathbf{x}}\mathbf{y}}(\omega)\mathbf{y}(\omega) \\ &= \Delta\mathbf{T}_{\hat{\mathbf{x}}\mathbf{y}}(\omega)\mathbf{H}_{\mathbf{y}\mathbf{p}}(\omega)\mathbf{p}(\omega) + \Delta\mathbf{T}_{\hat{\mathbf{x}}\mathbf{y}}(\omega)\mathbf{H}_{\mathbf{y}\mathbf{w}}(\omega)\mathbf{w}(\omega) + \Delta\mathbf{T}_{\hat{\mathbf{x}}\mathbf{y}}(\omega)\mathbf{v}(\omega)\end{aligned} \tag{30}$$

$$\begin{aligned}\Delta\hat{\mathbf{p}}(\omega) = \hat{\mathbf{p}}(\omega) - \hat{\mathbf{p}}_e(\omega) &= \Delta\mathbf{T}_{\hat{\mathbf{p}}\mathbf{y}}(\omega)\mathbf{y}(\omega) \\ &= \Delta\mathbf{T}_{\hat{\mathbf{p}}\mathbf{y}}(\omega)\mathbf{H}_{\mathbf{y}\mathbf{p}}(\omega)\mathbf{p}(\omega) + \Delta\mathbf{T}_{\hat{\mathbf{p}}\mathbf{y}}(\omega)\mathbf{H}_{\mathbf{y}\mathbf{w}}(\omega)\mathbf{w}(\omega) + \Delta\mathbf{T}_{\hat{\mathbf{p}}\mathbf{y}}(\omega)\mathbf{v}(\omega)\end{aligned} \tag{31}$$

where $\Delta\mathbf{T}_{\hat{\mathbf{x}}\mathbf{y}}(\omega) = \mathbf{T}_{\hat{\mathbf{x}}\mathbf{y}}(\omega) - \mathbf{T}_{\hat{\mathbf{x}}\mathbf{y}}^e(\omega)$ and $\Delta\mathbf{T}_{\hat{\mathbf{p}}\mathbf{y}}(\omega) = \mathbf{T}_{\hat{\mathbf{p}}\mathbf{y}}(\omega) - \mathbf{T}_{\hat{\mathbf{p}}\mathbf{y}}^e(\omega)$. The result is similar to the previous derivation in Section 2.3. Also here, a transformation of the input $\mathbf{p}(\omega)$ drives the estimate deltas (in addition to $\mathbf{w}$ and $\mathbf{v}$). In Section 3, attention is devoted to the transfer functions $\Delta\mathbf{T}_{\hat{\mathbf{x}}\mathbf{y}}(\omega)\mathbf{H}_{\mathbf{y}\mathbf{p}}(\omega)$ and $\Delta\mathbf{T}_{\hat{\mathbf{p}}\mathbf{y}}(\omega)\mathbf{H}_{\mathbf{y}\mathbf{p}}(\omega)$ to study this transformation in the frequency domain.

2.5 Alternative expressions for model error propagation

Since the input estimation is unbiased, the filter transfer function $\mathbf{T}_{\hat{\mathbf{p}}\mathbf{y}}(\omega)$ neutralizes the system input-output transfer function $\mathbf{H}_{\mathbf{y}\mathbf{p}}(\omega)$:

$$\mathbf{T}_{\hat{\mathbf{p}}\mathbf{y}}(\omega)\mathbf{H}_{\mathbf{y}\mathbf{p}}(\omega) = \mathbf{I} \tag{32}$$

The same principle is true for the erroneous system:

$$\mathbf{T}_{\hat{\mathbf{p}}\mathbf{y}}^e(\omega)\mathbf{H}_{\mathbf{y}\mathbf{p}}^e(\omega) = \mathbf{I} \tag{33}$$

Eq. (29) may be repeated as:

$$\hat{\mathbf{p}}_e(\omega) = \mathbf{T}_{\hat{\mathbf{p}}\mathbf{y}}^e(\omega)\mathbf{y}(\omega) = \mathbf{T}_{\hat{\mathbf{p}}\mathbf{y}}^e(\omega)\big(\mathbf{H}_{\mathbf{y}\mathbf{p}}(\omega)\mathbf{p}(\omega) + \mathbf{H}_{\mathbf{y}\mathbf{w}}(\omega)\mathbf{w}(\omega) + \mathbf{v}(\omega)\big) \tag{34}$$

If the noise terms $\mathbf{w}$ and $\mathbf{v}$ are disregarded for simplicity, and the relation $\mathbf{T}_{\hat{\mathbf{p}}\mathbf{y}}^e = \mathbf{T}_{\hat{\mathbf{p}}\mathbf{y}} - \Delta\mathbf{T}_{\hat{\mathbf{p}}\mathbf{y}}$ is introduced, the following expression comes out:

$$\hat{\mathbf{p}}_e(\omega) = \big(\mathbf{T}_{\hat{\mathbf{p}}\mathbf{y}}(\omega)\mathbf{H}_{\mathbf{y}\mathbf{p}}(\omega) - \Delta\mathbf{T}_{\hat{\mathbf{p}}\mathbf{y}}(\omega)\mathbf{H}_{\mathbf{y}\mathbf{p}}(\omega)\big)\mathbf{p}(\omega) = \big(\mathbf{I} - \Delta\mathbf{T}_{\hat{\mathbf{p}}\mathbf{y}}(\omega)\mathbf{H}_{\mathbf{y}\mathbf{p}}(\omega)\big)\mathbf{p}(\omega) \tag{35}$$

If instead the relation $\mathbf{H}_{\mathbf{y}\mathbf{p}} = \mathbf{H}_{\mathbf{y}\mathbf{p}}^e + \Delta\mathbf{H}_{\mathbf{y}\mathbf{p}}$ is used, the following alternative is found:

$$\hat{\mathbf{p}}_e(\omega) = \big(\mathbf{T}_{\hat{\mathbf{p}}\mathbf{y}}^e(\omega)\mathbf{H}_{\mathbf{y}\mathbf{p}}^e(\omega) + \mathbf{T}_{\hat{\mathbf{p}}\mathbf{y}}^e(\omega)\Delta\mathbf{H}_{\mathbf{y}\mathbf{p}}(\omega)\big)\mathbf{p}(\omega) = \big(\mathbf{I} + \mathbf{T}_{\hat{\mathbf{p}}\mathbf{y}}^e(\omega)\Delta\mathbf{H}_{\mathbf{y}\mathbf{p}}(\omega)\big)\mathbf{p}(\omega) \tag{36}$$

This reformulation is particularly useful since it means the propagation of errors can be directly linked to the perturbation $\Delta\mathbf{H}_{\mathbf{y}\mathbf{p}}(\omega)$ (which is quite easily expressed and understood) rather than $\Delta\mathbf{T}_{\hat{\mathbf{p}}\mathbf{y}}(\omega)$ (which has a rather cumbersome definition due to its inverse nature).

3 Numerical example

3.1 System with four degrees of freedom

The mass-spring system in Fig. 1 with 4 DOFs is used as a numerical example. Table 1 presents both the true and erroneous values of the spring stiffnesses and masses, with slight errors introduced at the level of $2.5 - 10\%$.

Modal properties are computed for both systems, as shown in Table 2. Errors in the natural frequencies are around $2.2 - 4.5\%$, where the first three modes exhibit an undershoot while the last mode is overshot. The mode shapes for both system models are shown in Fig. 2, where minor differences are visible. However, their correspondence quantified by the modal assurance criterion (MAC) [24], remains consistently above 0.98 for all modes.

For simplicity, proportional damping $\mathbf{C} = \alpha\mathbf{M} + \beta\mathbf{K}$ is used. The Rayleigh damping coefficients α and β are listed in Table 1 for both models. As shown in Table 2, the true damping ratios fall within the range of 0.65% to 1.05%, whereas the erroneous damping ratios are larger by a factor of $1.4 - 1.9$ since both the mass matrix, stiffness matrix, and the coefficients α and β are misspecified. This level of error is not unusual given the inherent uncertainties in damping characteristics in many civil structures.
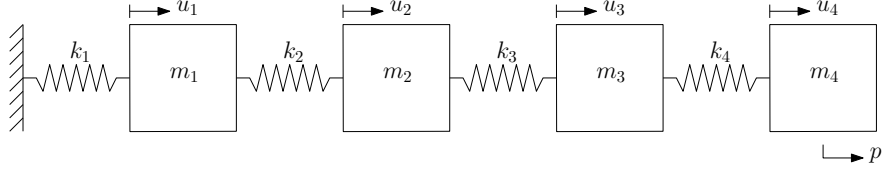

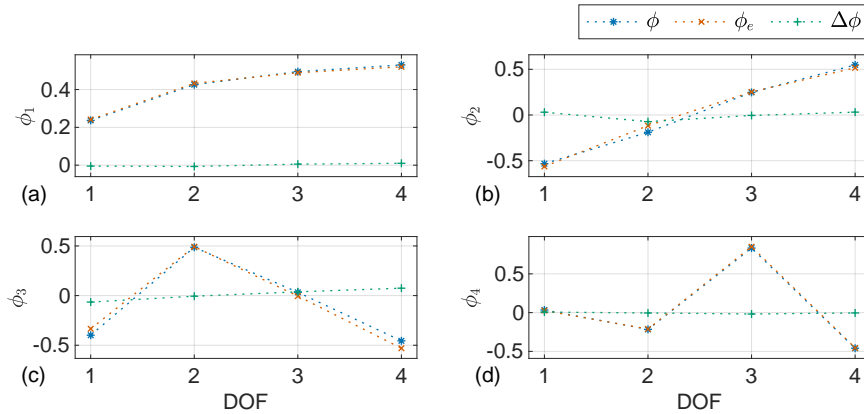Figure 1: Linear system with four degrees of freedom.

Figure 2: Mode shapes of the true and erroneous model.

Table 1: Mechanical properties: spring stiffnesses k_i in N/m, lumped masses m_i in kg, and Rayleigh damping coefficients α and β.

	k_1	k_2	k_3	k_4	m_1	m_2	m_3	m_4	α	β
True	10.00	10.00	15.00	15.00	2.00	2.00	1.00	1.00	$1.0 \cdot 10^{-2}$	$3.0 \cdot 10^{-3}$
Erroneous	9.00	9.00	16.00	15.00	2.05	2.05	0.975	0.975	$2.0 \cdot 10^{-2}$	$4.0 \cdot 10^{-3}$
Difference [%]	-10.00	-10.00	6.67	0.00	2.50	2.50	-2.50	-2.50	—	—

The system is loaded in DOF 4, where a force history of 10 minutes is generated from the following one-sided

Table 2: Modal properties: undamped natural frequencies ω_i in rad/s and damping ratios ξ_i in %.

	ω_1	ω_2	ω_3	ω_4	ξ_1	ξ_2	ξ_3	ξ_4
True	1.00	2.87	4.01	6.49	0.65	0.60	0.73	1.05
Erroneous	0.96	2.81	3.90	6.64	1.23	0.92	1.04	1.48
Difference [%]	-4.50	-2.18	-2.66	2.28	90.37	51.77	42.78	40.70
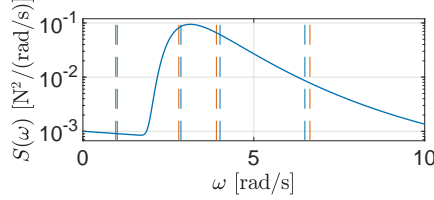
Figure 3: Spectral density of the input force.

spectral density function:

$$S(\omega) = \frac{100}{\omega^5} \cdot \exp\left(-\frac{5}{4}\left(\frac{\omega}{0.5 \cdot 2\pi}\right)^{-4}\right) + 0.001 \exp\left(-0.1\omega\right) \tag{37}$$

This spectral density is shown in Fig. 3, and is a Pierson-Moskowitz-type wave spectrum plus a small exponential term. The frequency content of the force is concentrated mainly in the range $2 - 8$ rad/s, but excites all the natural frequencies to various extents. A time step of $\Delta t = 0.02$ s is used. The output vector $\mathbf{y} = [\ddot{u}_4, u_2]^\mathrm{T}$ is considered, i.e. an acceleration collocated with the load in DOF 4, and a displacement in DOF 2. The displacement output is required in order to stabilize the joint input and state estimation, which cannot reach a steady state solely with acceleration outputs. Note that the output data is always generated from the true model, whereas the estimation is performed using both the true and the erroneous models to gauge the difference in their performances.

The transfer function $\mathbf{H}_{\mathbf{yp}}(\omega)$ from Eq. (6) is shown in Fig. 4 for both models. In this and subsequent frequency-domain plots, vertical lines are indicated for the following important parameters:

- Blue dashed line: true natural frequency
- Red dashed line: erroneous natural frequency
- Blue dotted line: true anti-resonance frequency
- Red dotted line: erroneous anti-resonance frequency

It is evident that modeling errors cause perturbations in both the natural frequencies and the anti-resonance frequencies. The implications of these perturbations are important and will be discussed later. Note that the transfer function for the acceleration output in Fig. 4 has three anti-resonance frequencies, but for the displacement there is only one. This is not a result of the output type, but the location: outputs collocated with the input will have an anti-resonance frequency between each resonance frequency, but this is not always the case for non-collocation [18].

Measurement white noise $\mathbf{v}$ is added to the simulation outputs, according to $\mathbf{R} = 10^{-3} \cdot \mathbf{I}$. Thus, both the acceleration and displacement output have the same noise statistics; the effect of heterogeneous covariance is discussed later. For simplicity, the process noise $\mathbf{w}$ is not applied and therefore both $\mathbf{Q}$ and $\mathbf{S}$ are set to zero.

3.2 State estimation

First, the problem of pure state estimation using the Kalman filter in Eq. (11)$-$(17) is considered. The resulting estimates for the displacement states are shown in Fig. 5. The estimate from the true model yields
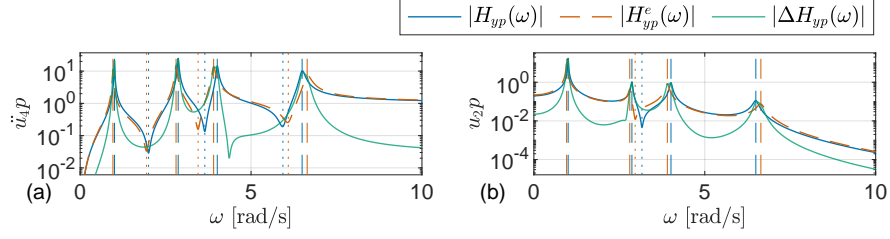
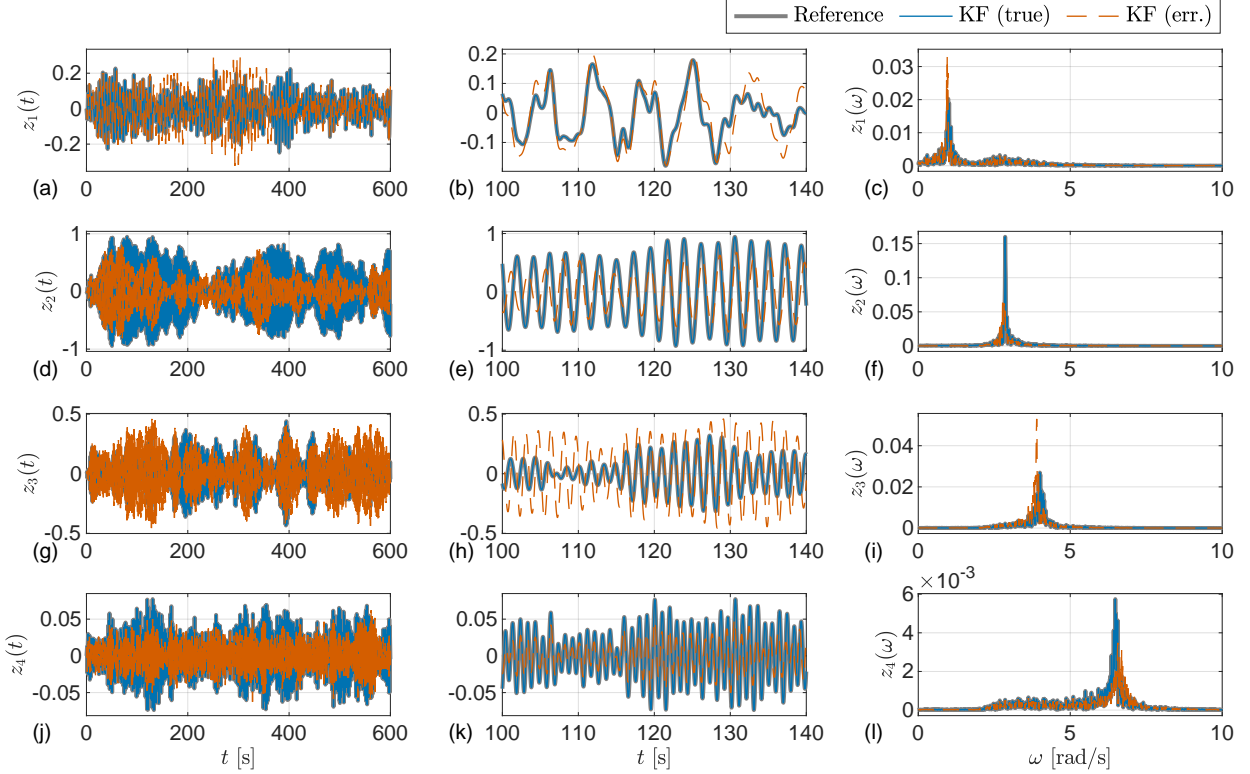Figure 4: Input-to-output transfer function of the true and erroneous model.

Figure 5: Modal state estimates from the Kalman filter.

an almost perfect match to the reference. This is hardly surprising since the input force is fully known, and there is no additional white noise excitation. On the other hand, the erroneous estimate contains, as expected, obvious inaccuracies. The erroneous estimate peaks at incorrect frequencies.

Since the process noise covariance is $\mathbf{Q} = \mathbf{0}$, there is no room for the Kalman filter to correct the dynamics of the system, and it largely acts as a deterministic forward model where the input force is applied and the response is propagated step-by-step in time. In this case, the information from the output bears no additional information. Therefore, the term $\mathbf{T}_{\hat{\mathbf{x}}\mathbf{y}}(\omega)$ from Eq. (21) is approximately zero (as is $\mathbf{T}^e_{\hat{\mathbf{x}}\mathbf{y}}(\omega)$). Consequently, the term $\Delta\mathbf{T}_{\hat{\mathbf{x}}\mathbf{y}}(\omega)\mathbf{H}_{\mathbf{y}\mathbf{p}}(\omega) + \Delta\mathbf{T}_{\hat{\mathbf{x}}\mathbf{p}}$ from Eq. (25), which is shown in Fig. 6, largely reflects the delta in the input-to-states transfer function $\mathbf{H}_{\mathbf{x}\mathbf{p}}(\omega)$ between the true and erroneous model.

If $\mathbf{Q} > \mathbf{0}$, a different scenario would play out wherein the process noise would (sub-optimally) compensate for the model errors. In practical problems, using $\mathbf{Q} = \mathbf{0}$ is rarely a good choice since there could always be some stochastic background excitation or minor errors in the continuous-to-discrete transformation of the state-space model, such that the state-equation Eq. (1) rarely is without noise (even if $\mathbf{A}$ and $\mathbf{B}$ are error-free). The case of pure state estimation with $\mathbf{Q} = \mathbf{0}$ is therefore here shown as an initial example and a baseline for comparison with the case of joint input and state estimation.
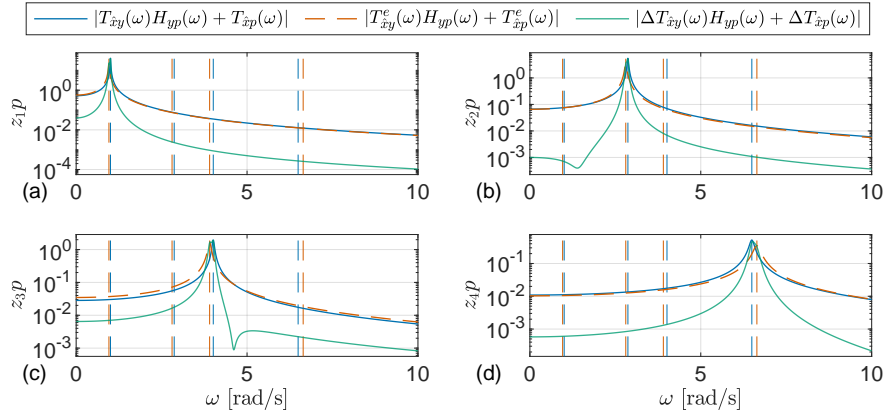
Figure 6: Transfer function of the force-to-state-estimate for the Kalman filter.

3.3 Input and state estimation

The next presented problem is the joint input and state estimation [2]. The analysis is the same as in Section 3.2, except that the force is treated as unknown. Note that the force location is assumed to be known (still in DOF 4). The state estimates are shown in Fig. 7 for the time and frequency domain. Contrary to the Kalman filter (Fig. 5), some of the modal states (e.g. mode 2 and 4) are estimated quite well even for the erroneous model. This improvement in state estimation accuracy comes at the cost of the identified force, which will have to compensate for the model errors. Still, for modes 1 and 3 in particular, the state estimates contain significant frequency errors, meaning that the error compensation by the force is far from perfect.

The observed frequency errors in Fig. 7 can be explained by Figs. 8 and 9, which show the error propagation in the frequency domain. Fig. 9 illustrates that errors arise not only at a mode's own natural frequency but also across the entire frequency range, particularly at resonance and anti-resonance frequencies. These results point to the possible usefulness of these frequency-domain markers to detect model errors in a practical situation. The observation of spurious peaks at the anti-resonance frequencies has already been discussed in e.g. [25], where it was shown the importance of correctly representing these frequencies due to quasi-static response behaviour when reduced-order modal models are employed. In the present example, no modal truncation is used, and so no quasi-static correction is needed.

If modal loads were identified rather than concentrated forces, the state estimates would improve, but this would also require additional acceleration outputs (equal to the number of modal loads). A similar situation was discussed in [26], where it was also studied the influence of misspecifying the position of the force, which is also a form of model error where the allocation matrix $\mathbf{S_p}$ is wrong, and consequently error compensations also take will place in the form of so-called equivalent forces.

Fig. 10 shows the input estimates. The estimate for the true model reconstructs the force quite well, but the erroneous model estimate exhibits spurious peaks (and valleys) across the frequency axis. It is obvious that these are related to the model errors and that the force compensates for what cannot be explained by the erroneous model predictions when compared to the output data.

As explained in the following, the observed errors can be more closely linked to the resonance and anti-resonance frequencies involved in the problem. Fig. 12 shows the absolute value of $\mathbf{I} - \Delta\mathbf{T_{\hat{p}y}}(\omega)\mathbf{H_{yp}}(\omega)$ from Eq. (35). Here, a value of 1 is optimal and indicates no distortion of the force due to model errors, whereas a lower or higher value indicates deflation or inflation at a given frequency.
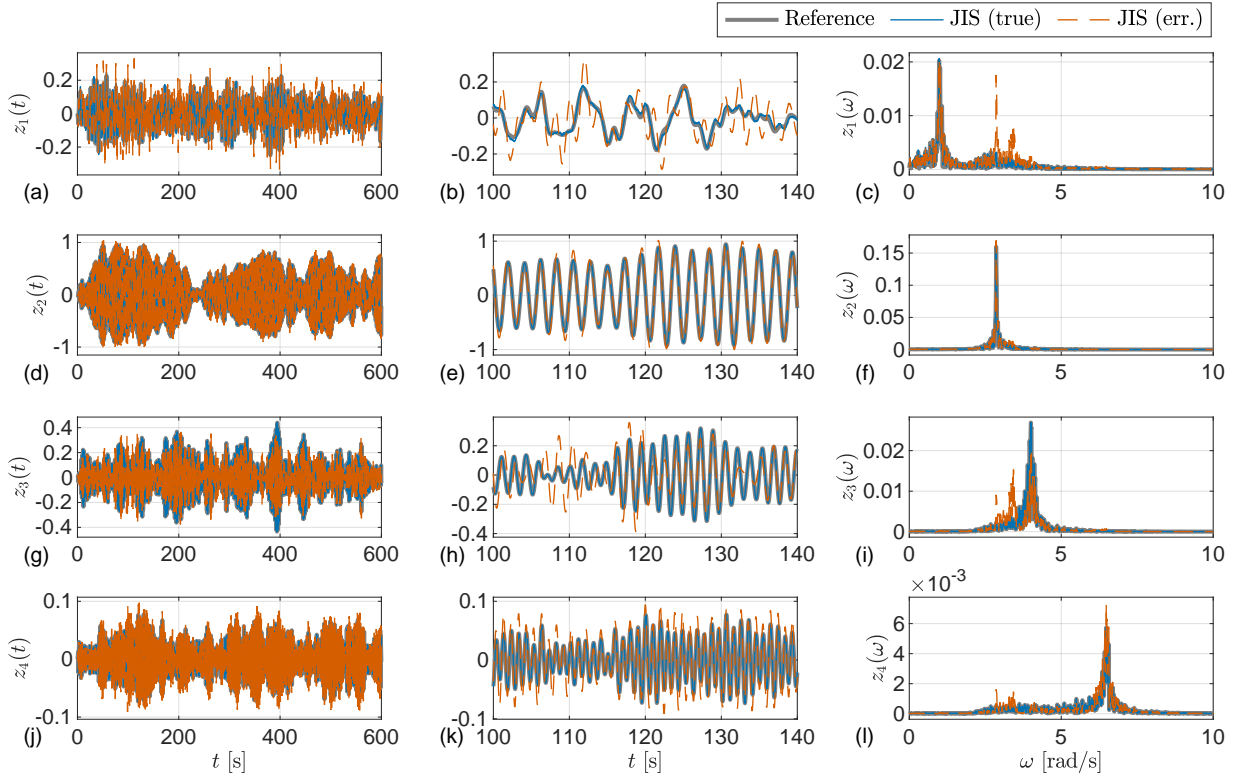
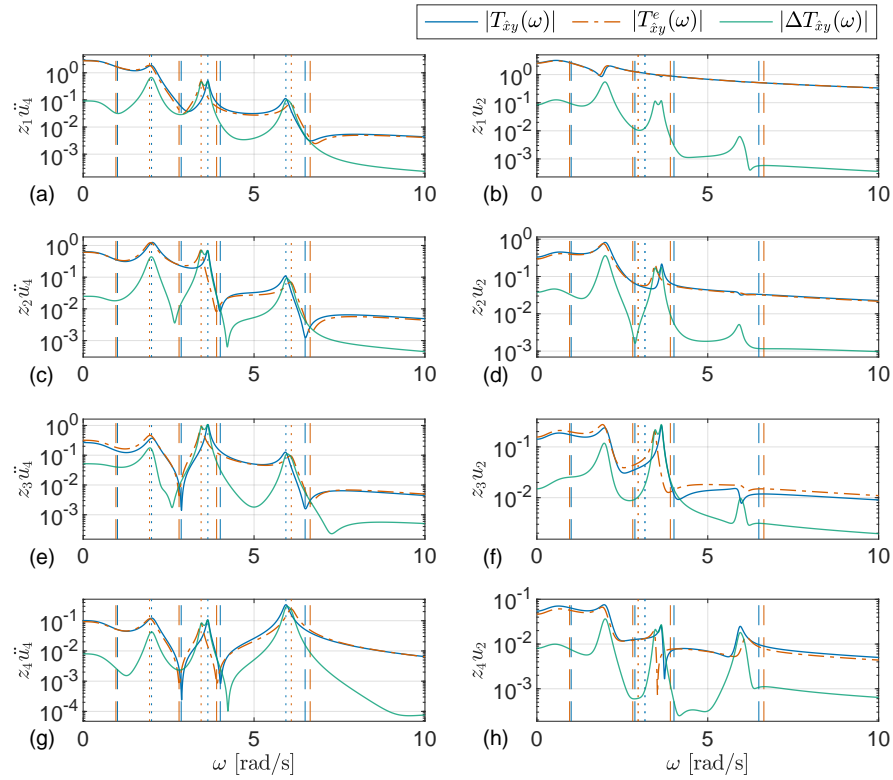Figure 7: Modal state estimates from the joint input and state estimation.

Figure 8: Transfer function of the output-to-state-estimate for the joint input and state estimation.
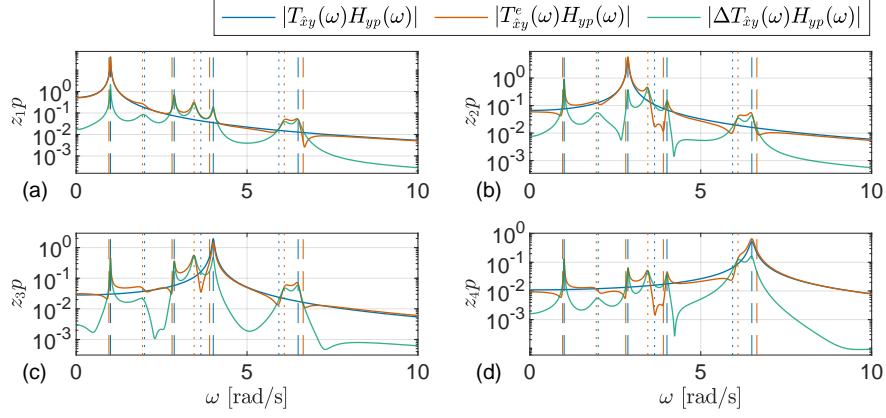
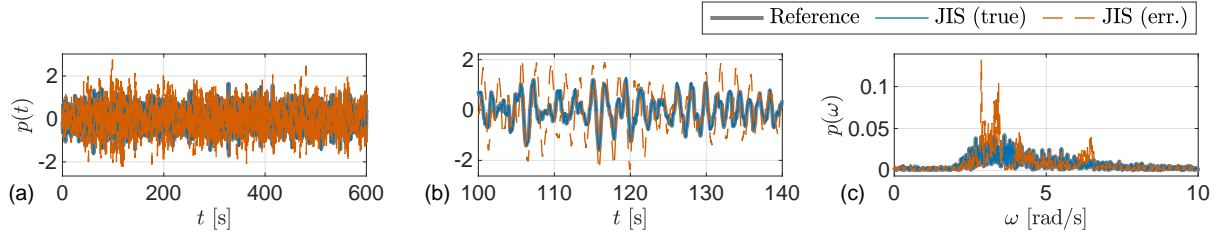Figure 9: Transfer function of the input-to-state-estimate for the joint input and state estimation.

Figure 10: Input estimate from the joint input and state estimation.
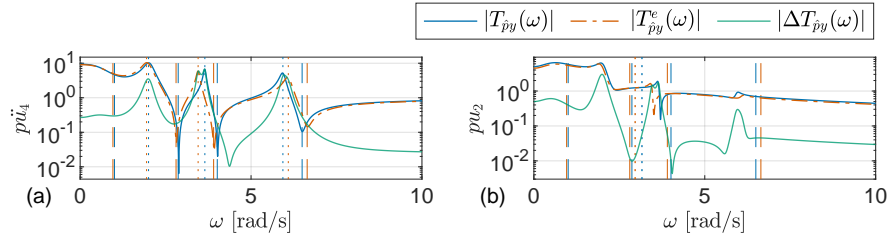

Figure 11: Transfer function of the output-to-input-estimate for the joint input and state estimation.
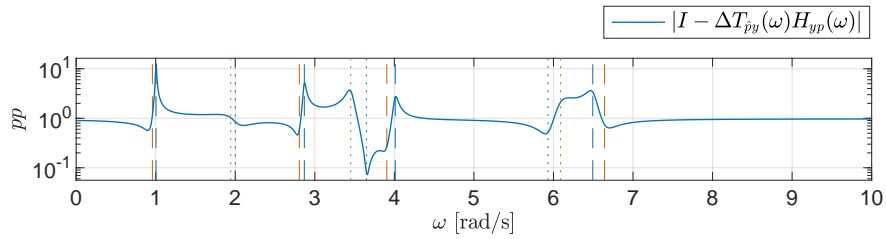

Figure 12: Transfer function illustrating the distortion of the input estimate, where deviations from a value of unity indicate a deflation or inflation of the force.

Several peaks and valleys are observed in Fig. 12: force inflations tend to occur at the resonance frequencies of the *true* system and the anti-resonance frequencies of the *erroneous* system, while deflations are found at resonance frequencies of the *erroneous* system and the anti-resonance frequencies of the *true* system. This behaviour can be traced back to the curves of $\Delta\mathbf{T}_{\hat{\mathbf{p}}\mathbf{y}}(\omega)$ in Fig. (11) and $\mathbf{H}_{\mathbf{y}\mathbf{p}}(\omega)$ in Fig. (4) (or, alternatively, to $\mathbf{T}_{\hat{\mathbf{p}}\mathbf{y}}^{e}(\omega)$ and $\Delta\mathbf{H}_{\mathbf{y}\mathbf{p}}(\omega)$ since Eq. (36) was an equivalent formulation to Eq. (35)). These listed characterizations of force inflation and deflations indicate general trends. The exact picture of the input estimate frequency distortions will depend on the total influence of all modal parameter errors. Additionally, these findings highlight an important limitation in error detection for practical applications: while it is possible to compute the erroneous resonance and anti-resonance frequencies, the true values can be unknown or at least uncertain.

Generally, it can be said that any form of model discrepancies (modal parameter errors, effects due to reduced-order truncation, unmodelled dynamics, or other types of model-vs-reality mismatch) will lead to a misrepresentation of the systems input-to-output transfer function, which inevitably propagates to the inversion of the system. The extent to which any mismatch will significantly corrupt the results is case-specific, however.

3.4   Sensitivity to noise covariance values

While the formulas derived in Sections 2.3 and 2.4 are general, the results presented in the numerical example are specific to the given system, model errors, sensor locations, and the adopted noise covariance matrices. It is here examined the influence of measurement noise statistics by considering two additional cases: $\mathbf{R} = \mathrm{diag}(10^{-6}, 10^{-3})$ and $\mathbf{R} = \mathrm{diag}(10^{-3}, 10^{-6})$. These cases correspond to scenarios where either the acceleration output $\ddot{u}_4$ or the displacement output u_2 is assigned higher confidence (i.e., lower noise variance by a factor of 10^3).

Fig. 13 shows the frequency-domain distortion of the input estimate $(\mathbf{I} - \Delta\mathbf{T}_{\hat{\mathbf{p}}\mathbf{y}}(\omega)\mathbf{H}_{\mathbf{y}\mathbf{p}}(\omega))$ for the two new cases compared to the original case where $\mathbf{R} = \mathrm{diag}(10^{-3}, 10^{-3})$. While the overall characteristics of the curves remain similar for all three cases, the scaling of the peaks and valleys vary significantly. This variation results from a combination of factors: *i*) the differing information carried by the two outputs (one being a displacement and the other an acceleration) and *ii*) the mode shape error $\Delta\mathbf{\Phi}$ differing at the two sensor locations, and the propagation of these errors depends on the relative weighting resulting from the specified noise variances.

The results further raise the question of how sensor locations and sensor types can be robustly designed to reduce the impact of model errors on joint input and state estimation. Addressing this issue is left for future research.
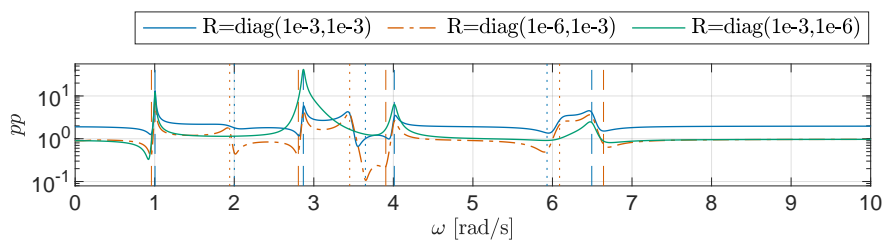

Figure 13: Transfer function showing the distortion of the input estimate for different levels of noise for the two outputs.

4 Conclusions

This study has investigated the impact of model errors on input and state estimation within structural dynamic systems. The considered model errors were perturbations in the modal parameters in the state-space models. Through frequency-domain analysis of the transfer functions of the Bayesian filters (such as the Kalman filter), it was shown that model errors lead to spurious frequency components in the estimates. The frequency distribution of these estimate errors can be linked to the resonance and anti-resonance frequencies of both the true model and the erroneous model. These analytical insights were validated through a numerical example.

The tools derived in this contribution can be used to characterize the impact and propagation of model errors in a general theoretical framework, which may be useful in the further development of techniques to mitigate the adverse effects of model errors, thereby enhancing the reliability of input and state estimation.

References

[1] R. E. Kalman, "A new approach to linear filtering and prediction problems," *Journal of basic Engineering*, vol. 82, no. 1, pp. 35–45, 1960.

[2] E. Lourens, C. Papadimitriou, S. Gillijns, E. Reynders, G. De Roeck, and G. Lombaert, "Joint input-response estimation for structural systems based on reduced-order models and vibration data from a limited number of sensors," *Mechanical Systems and Signal Processing*, vol. 29, pp. 310–327, 2012.

[3] E. Lourens, E. Reynders, G. De Roeck, G. Degrande, and G. Lombaert, "An augmented Kalman filter for force identification in structural dynamics," *Mechanical Systems and Signal Processing*, vol. 27, pp. 446–460, 2012.

[4] S. E. Azam, E. Chatzi, and C. Papadimitriou, "A dual Kalman filter approach for state estimation via output-only acceleration measurements," *Mechanical Systems and Signal Processing*, vol. 60, pp. 866–886, 2015.

[5] K. Maes, A. Smyth, G. De Roeck, and G. Lombaert, "Joint input-state estimation in structural dynamics," *Mechanical Systems and Signal Processing*, vol. 70–71, pp. 445–466, 2016.

[6] O. Sedehi, C. Papadimitriou, D. Teymouri, and L. S. Katafygiotis, "Sequential Bayesian estimation of state and input in dynamical systems using output-only measurements," *Mechanical Systems and Signal Processing*, vol. 131, pp. 659–688, 2019.

[7] D. Teymouri, O. Sedehi, L. S. Katafygiotis, and C. Papadimitriou, "A Bayesian Expectation-Maximization (BEM) methodology for joint input-state estimation and virtual sensing of structures," *Mechanical Systems and Signal Processing*, vol. 169, p. 108602, 2022.

[8] K. Erazo, D. Sen, S. Nagarajaiah, and L. Sun, "Vibration-based structural health monitoring under changing environmental conditions using kalman filtering," *Mechanical systems and signal processing*, vol. 117, pp. 1–15, 2019.

[9] H. Heffes, "The effect of erroneous models on the Kalman filter response," *IEEE Transactions on Automatic Control*, vol. 11, no. 3, pp. 541–543, 1966.

[10] T. M. Hamill and J. S. Whitaker, "Accounting for the error due to unresolved scales in ensemble data assimilation: A comparison of different approaches," *Monthly weather review*, vol. 133, no. 11, pp. 3132–3147, 2005.

[11] G. Evensen, "The ensemble Kalman filter: Theoretical formulation and practical implementation," *Ocean dynamics*, vol. 53, pp. 343–367, 2003.

[12] A. Corigliano and S. Mariani, "Parameter identification in explicit structural dynamics: performance of the extended kalman filter," *Computer methods in applied mechanics and engineering*, vol. 193, no. 36-38, pp. 3807–3835, 2004.

[13] F. Naets, J. Croes, and W. Desmet, "An online coupled state/input/parameter estimation approach for structural dynamics," *Computer Methods in Applied Mechanics and Engineering*, vol. 283, pp. 1167–1188, 2015.

[14] M. Impraimakis and A. W. Smyth, "An unscented kalman filter method for real time input-parameter-state estimation," *Mechanical Systems and Signal Processing*, vol. 162, p. 108026, 2022.

[15] R. Mehra, "On the identification of variances and adaptive kalman filtering," *IEEE Transactions on automatic control*, vol. 15, no. 2, pp. 175–184, 1970.

[16] K. Myers and B. Tapley, "Adaptive sequential estimation with unknown noise statistics," *IEEE transactions on automatic control*, vol. 21, no. 4, pp. 520–523, 1976.

[17] Z.-F. Fu and J. He, *Modal analysis*.   Elsevier, 2001.

[18] D. J. Ewins, *Modal testing: theory, practice and application*.   John Wiley & Sons, 2009.

[19] G. W. Skingle, "Structural dynamic modification using experimental data," Ph.D. dissertation, University of London, 1989.

[20] F. Wahl, G. Schmidt, and L. Forrai, "On the significance of antiresonance frequencies in experimental structural analysis," *Journal of Sound and Vibration*, vol. 219, no. 3, pp. 379–394, 1999.

[21] Y. Bulut and O. Bayat, "Kalman filtering with model uncertainties," in *Topics in Modal Analysis I, Volume 5: Proceedings of the 30th IMAC, A Conference on Structural Dynamics, 2012*.   Springer, 2012, pp. 447–455.

[22] Q. Ge, T. Shao, Z. Duan, and C. Wen, "Performance analysis of the kalman filter with mismatched noise covariances," *IEEE Transactions on Automatic Control*, vol. 61, no. 12, pp. 4014–4019, 2016.

[23] F. L. Lewis, L. Xie, and D. Popa, *Optimal and robust estimation: with an introduction to stochastic control theory*, 2nd ed.   Florida, USA: Taylor & Francis Group, 2007.

[24] R. J. Allemang, "The modal assurance criterion–twenty years of use and abuse," *Sound and Vibration*, vol. 37, no. 8, pp. 14–23, 2003.

[25] K. Maes and G. Lombaert, "The influence of out-of-band modes in system inversion," *Mechanical Systems and Signal Processing*, vol. 115, pp. 173–187, 2019.

[26] E. Lourens and D. Fallais, "Full-field response monitoring in structural systems driven by a set of identified equivalent forces," *Mechanical Systems and Signal Processing*, vol. 114, pp. 106–119, 2019.